NUCL SCI TECH (2019) 30:52
https://doi.org/10.1007/s41365-019-0564-8

Quantitative energy-dispersive X-ray fluorescence analysis for unknown samples using full-spectrum least-squares regression

Yong-Li Liu[1] · Qing-Xian Zhang[1] · Jian Zhang[1] · Hai-Tao Bai[1] · Liang-Quan Ge[1]

Received: 3 May 2018 / Revised: 8 August 2018 / Accepted: 10 August 2018 / Published online: 22 February 2019
© China Science Publishing & Media Ltd. (Science Press), Shanghai Institute of Applied Physics, the Chinese Academy of Sciences, Chinese Nuclear Society and Springer Nature Singapore Pte Ltd. 2019

Abstract The full-spectrum least-squares (FSLS) method is introduced to perform quantitative energy-dispersive X-ray fluorescence analysis for unknown solid samples. Based on the conventional least-squares principle, this spectrum evaluation method is able to obtain the background-corrected and interference-free net peaks, which is significant for quantization analyses. A variety of analytical parameters and functions to describe the features of the fluorescence spectra of pure elements are used and established, such as the mass absorption coefficient, the G_i factor, and fundamental fluorescence formulas. The FSLS iterative program was compiled in the C language. The content of each component should reach the convergence criterion at the end of the calculations. After a basic theory analysis and experimental preparation, 13 national standard soil samples were detected using a spectrometer to test the feasibility of using the algorithm. The results show that the calculated contents of Ti, Fe, Ni, Cu, and Zn have the same changing tendency as the corresponding standard content in the 13 reference samples. Accuracies of 0.35% and 14.03% are obtained, respectively, for Fe and Ti, whose standard concentrations are 8.82% and 0.578%, respectively. However, the calculated results of trace elements (only tens of μg/g) deviate from the standard values. This may be because of measurement accuracy and mutual effects between the elements.

Keywords Energy-dispersive X-ray fluorescence analysis · Full-spectrum least-squares method · Effective atomic number · Mass attenuation coefficient · Fundamental parameter method

1 Introduction

Energy-dispersive X-ray fluorescence (EDXRF) is an analytical method for determining the concentration of micro and major elements in different matrices. This technology is widely used in pharmaceutical analysis, antique authentication, and the exploration of mineral resources because of its rapid and nondestructive analysis process [1]. However, calibrating the efficiency of the instrument and matrix effect correction are the most realistically difficult problems in EDXRF. Many studies focusing on these two problems have been conducted. Since the 1950s, the mutual impact coefficient method and the fundamental parameter method (FPM) have been the main methods used in X-ray fluorescence analyses. The former consists in calibrating efficiency with standard samples to solve the problem of overlapping-peak peeling, but the X-ray fluorescence spectrometer has to be rescaled when there are large matrix differences in the sample [2]. The FPM is a widely used method based on physical parameters. It can effectively reduce the absorption and enhancement effects. The major advantage of the FPM is the minimum number of standard samples required for efficiency calibration [3–5]. However, most measurements

This work was supported by the National Key R&D Project of China (No. 2017YFC0602100), the National Natural Science Foundation of China (No. 41774147) and Sichuan Science and Technology Support Program (No. 2015GZ0272).

✉ Qing-Xian Zhang
Zhangqingxian06@cdut.cn

[1] The College of Applied Nuclear Technology and Automation Engineering, Chengdu University of Technology, Chengdu 610059, China

based on the FPM are developed for wavelength-dispersive X-ray fluorescence (WDXRF) analysis [6–9]. By comparison, the ability to carry out in situ measurement works is one of the major advantages of EDXRF. In conventional EDXRF, elements with an atomic number below 19 are commonly difficult to analyze in the field. Thus, a "dark matrix" must exist in the sample. To correct for the variations caused by the matrix effect, the backscatter fundamental parameter method was proposed and developed [10, 11]. In addition, several methods were developed for EDXRF analysis, which can be referred to in a previous review [12]. In recent years, using an effective atomic number Z_{eff} as a representative of the "dark matrix" has become the prevailing approach, and this parameter has also been studied in our previous works [13, 14].

Usually, the net characteristic X-ray intensity of each element is derived once the EDXRF spectrum is taken, and then, the element concentration is calculated via the FPM [15]. This independent quantitative method has proven to be workable. However, it remains a complex and time-consuming process that requires a high degree of experience and knowledge from the instrument user [16]. The full-spectrum least-squares (FSLS) method is a multivariate calibration method that is able to, based on the conventional least-squares principle, increase the selectivity of matrix components and provide the possibility of detecting samples as outliers. Theoretically, it can deal with considerable peak overlaps owing to its lower dependence on the shape of predefined peak lines [17]. However, this multivariate calibration method is rarely applied in EDXRF except for near-infrared and infrared spectroscopic analytical studies [16–19]. Therefore, this paper explores the feasibility of using FSLS regression for the quantitative EDXRF determination of the concentration of micro and major elements, such as titanium (Ti), iron (Fe), nickel (Ni), copper (Cu), and zinc (Zn), which are common components in solid samples.

2 Theoretical descriptions

In EDXRF, the basic equations that relate the measured X-ray fluorescence intensity and the corresponding element composition were derived by Sherman and other authors [16, 20, 21]. When an X-ray beam irradiates the surface of the sample, the absorption and scattering of the original irradiated beam will occur along the trajectory path. The attenuation of the original irradiated beam caused by absorption and scattering not only is proportional to the incident X-ray intensity but also depends on the thickness, density, and the number of encountered atoms per unit cross section of the absorber. Based on this theory, the absorption of the original irradiated beam can be divided into three processes: I, II, and III, as shown in Fig. 1.

Process I represents the attenuation of the original X-ray (whose wavelength is λ and were produced by an X-ray tube) in the sample. Process II indicates the absorption of attenuated X-ray in the target element i in an infinitesimal volume. t is the incident depth of the X-ray along the surface normal. Element i, whose weight concentration is C_i, emits characteristic X-ray after being excited, the magnitude of which depends on the excitation factor (E_i). E_i is closely related to the jump ratio (J_i) for the absorption edge, transition probability (f_i), and fluorescence yield (w_i), which can be expressed as follows [21]:

$$E_i = J_i f_i w_i. \tag{1}$$

These characteristic X-rays are radiated evenly in all directions and are then attenuated by being absorbed by matter in process III. Only the X-ray with a spatial solid angle of $\Omega/4\pi$ can enter the detector. Therefore, the primary fluorescence intensity $(S_{i,\lambda})$ for a line of element i can be expressed as follows [20]:

$$S_{i,\lambda} = (\Omega/4\pi)\varepsilon_i \csc\varphi_1 C_i E_i \int_{\lambda_{\min}}^{\lambda_{\text{abs},i}} \frac{u_{i,\lambda}}{u'_s + u''_s} I_\lambda \mathrm{d}\lambda, \tag{2}$$

$$u'_{\text{s}} = u_{\text{s},\lambda}\text{cosec}\varphi_1, \tag{3}$$

$$u''_{\text{s}} = u_{\text{s},\lambda_i}\text{cosec}\varphi_2. \tag{4}$$

Here, φ_1 is the angle between the central beam of the tube's radiation and the surface of the sample. φ_2 is the takeoff angle of the measured radiation from the sample. ε_i is the intrinsic detection efficiency of the characteristic X-ray

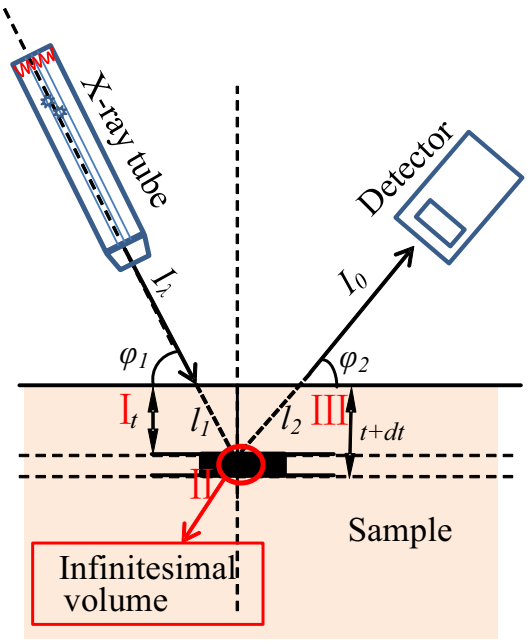

Fig. 1 (Color online) Measurement system structure for EDXRF

of element i. $\mu_{i,\lambda}$ is the mass absorption coefficient of element i for the original wavelength λ, and its unit is cm^2/g. Similarly, $\mu_{s,\lambda}$ is the mass absorption coefficient of the sample and μ_{s,λ_i} is its mass absorption coefficient for the characteristic X-ray wavelength λ_i. It should be noted that the original X-ray spectrum produced by the X-ray tube includes the continuous spectrum and the characteristic spectrum [2]. The former is the main X-ray source that excites the sample. For any given experimental conditions, there is no exact analytical expression to obtain the incident spectrum. Thus, the continuous integral over λ is divided into a number of intervals $\Delta\lambda_k$, and in this way, the spectral distribution of the original radiation can be obtained as follows:

$$\int_{\lambda_{\min}}^{\lambda_{\text{edge},i}} I_\lambda \mathrm{d}\lambda \rightarrow \sum_{\lambda_{\min}}^{\lambda_{\text{edge},i}} I_{\lambda_k}\Delta\lambda_k = I_0 \sum_{E_{\text{abs},i}}^{E_{\max}} \varphi(E).$$

Here, $\varphi(E)$ is the original X-ray spectral distribution, which can be simulated via Monte Carlo methods [22]. The simulation results for electrons ($\leq$ 30.3 keV) bombarding rhodium (Rh) target atoms obtained with the MCNP program are shown in Fig. 2.

In addition, I_0 is the total intensity of the original incident X-ray, which can be categorized, much like $\Omega/4\pi$, ε_i, and $\csc\varphi_1$, into a factor related to the structure of the instrument. The synthetic effect of these four parameters is taken as an important factor, G_i, which can be expressed as follows [20, 21]:

$$G_i = (\Omega/4\pi)\varepsilon_i \csc\varphi_1 I_0. \tag{5}$$

Thus, Eq. (2) can be simplified as follows:

$$S_{i,E} = G_i C_i E_i \sum_{E_{\text{abs},i}}^{E_{\max}} \frac{u_{i,E}}{u'_s + u''_s}\varphi(E), \tag{6}$$

where $S_{i,E}$, $u_{i,E}$, $u_{s,E}$, and u_{s,k_α} are equivalent to $S_{i,\lambda}$, $\mu_{i,\lambda}$, $\mu_{s,\lambda}$, and μ_{s,λ_i}, respectively. For multi-element samples,

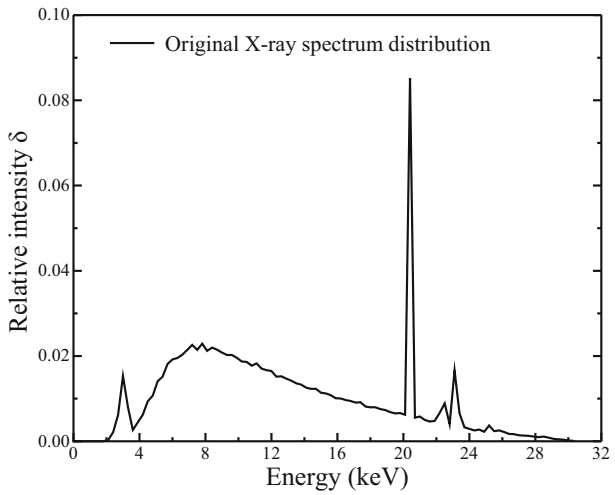

Fig. 2 Original X-ray spectral distribution obtained via Monte Carlo methods

when the excited wavelength of another interfering element j (whose concentration is C_j) in the matrix is less than the wavelength of the absorption edge of element i, secondary fluorescence will happen. This process also includes processes I, II, and III. The secondary fluorescence formula can be expressed as follows [20, 23]:

$$S_{ij,E} = S_{i,E} e_{ij,E} C_j, \tag{7}$$

where

$$e_{ij,E} = 0.5 E_j u_{i,E_j}\left(\frac{u_{j,E}}{u_{i,E}}\right)\left[\frac{1}{u'_s}\ln\left(1+\frac{us'}{u_{\text{s,E}_j}}\right)+\frac{1}{u''_{\text{s}}}\ln\left(1+\frac{us''}{u_{\text{s,E}_j}}\right)\right]. \tag{8}$$

Here, u_{i,E_j} and u_{s,E_j} are the mass absorption coefficient of element i and the mass absorption coefficient of the sample for the characteristic X-ray energy E_j of element j, respectively. The percentage of the tertiary X-ray fluorescence in the total detected intensity does not exceed 4%, even in the most extreme cases, and can be ignored in the calculations. Therefore, the detected intensity $I_{i,E}$ of the fluorescence radiation of element i in the sample can be expressed as the sum of the primary fluorescence intensity and the secondary fluorescence intensity [21].

$$I_{i,E} = S_{i,E} + S_{ij,E}. \tag{9}$$

Actually, in X-ray spectrum analyses, the count rate of one energy channel is not related only to the target element; it is also affected by other elements in the matrix. Therefore, the spectrum can be regarded as the sum of the contributions of a series of elements within the same matrix. Once the theoretical spectrum of a single element is obtained, the optimal response relationship between the content of that element and the detected X-ray spectrum can be established. Based on the fluorescence formulas, the calculated intensity is just a value equal to the total area of the detected X-ray peak for one element. Thus, the intensity at the peak position needs to be Gaussian-broadened [24] to the scale edge of the spectrometer, which is approximately 0–1023 channels. This can be described in the following procedure.

The Gaussian distribution prototype formula [25] is shown in the following.

$$f(x) = \frac{1}{\sigma\sqrt{2\pi}} e^{\frac{-(x-\mu)^2}{2\sigma^2}}. \tag{10}$$

Here, μ is the distribution expectation, which is the characteristic peak position in EDXRF spectral analysis. σ is the distribution's standard deviation, which is indispensable in the Gaussian-broadening process. Experimentally, nine kinds of single-element samples, namely potassium (K), calcium (Ca), titanium (Ti), iron (Fe), nickel (Ni), zinc (Zn), strontium (Sr), zirconium (Zr), and molybdenum

Table 1 Component proportions of the 45 standard samples (the mass of each sample was 0.05 kg)

No.	KCl	H_3BO_3	SiO_2	No.	CaO	H_3BO_3	SiO_2	No.	TiO_2	H_3BO_3	SiO_2
Component proportions (%) of the standard samples from No. 1 to No. 15											
1	0.19	28.58	71.23	6	0.14	28.57	71.29	11	0.17	28.57	71.26
2	0.96	28.57	70.47	7	0.70	28.57	70.73	12	0.83	28.57	70.59
3	1.91	28.57	69.52	8	1.40	28.57	70.03	13	1.68	28.62	69.69
4	9.54	28.57	61.89	9	6.99	28.57	64.43	14	8.35	28.56	63.09
5	19.08	28.57	52.35	10	13.99	28.57	57.44	15	16.69	28.57	54.74
No.	Fe_2O_3	H_3BO_3	SiO_2	No.	Ni	H_3BO_3	SiO_2	No.	ZnO	H_3BO_3	SiO_2
Component proportions (%) of the standard samples from No. 16 to No. 30											
16	0.14	28.57	71.29	21	0.11	28.57	71.32	26	0.13	28.57	71.31
17	0.71	28.57	70.72	22	0.51	28.57	70.93	27	0.62	28.57	70.81
18	1.43	28.57	70.00	23	1.00	28.57	70.43	28	1.24	28.57	70.18
19	7.15	28.57	64.28	24	5.00	28.57	66.43	29	6.23	28.57	65.20
20	14.30	28.57	57.13	25	10.00	28.57	61.43	30	12.47	28.57	58.97
No.	$SrCl_2{\cdot}6H_2O$	H_3BO_3	SiO_2	No.	ZrO_2	H_3BO_3	SiO_2	No.	MoO_3	H_3BO_3	SiO_2
Component proportions (%) of the standard samples from No. 31 to No. 45											
31	0.29	28.58	71.14	36	0.13	28.57	71.30	41	0.15	28.57	71.28
32	1.54	28.57	69.89	37	0.67	28.57	70.76	42	0.75	28.58	70.68
33	3.05	28.57	68.38	38	1.35	28.57	70.08	43	1.51	28.57	69.92
34	15.22	28.57	56.22	39	6.76	28.57	64.67	44	7.51	28.57	63.92
35	30.43	28.57	41.00	40	13.51	28.57	57.92	45	15.01	28.57	56.42

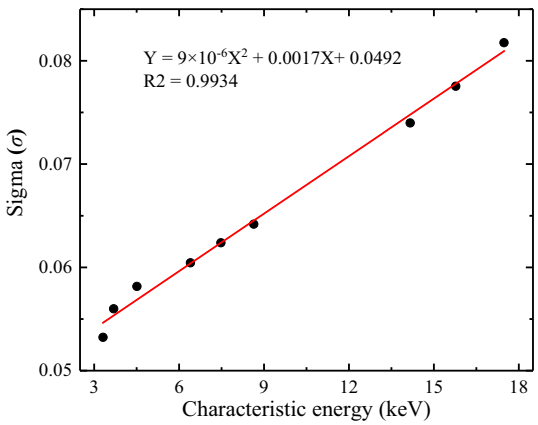

Fig. 3 (Color online) Relationship between σ and the characteristic energy of different elements

(Mo), were prepared, as given in Table 1 in the next section. The actual EDXRF spectra were Gaussian fitted with the OriginPro9 program, and then, the σ of each element's spectral line was obtained. The functional relationship between the characteristic energy and σ is shown in Fig. 3.

Once the σ of element i is obtained via interpolation through Eq. (10), the characteristic X-ray intensity $I_{i,E}$ can be Gaussian-broadened into 1023 energy channels: $(E_{i,0},\ E_{i,1},\ E_{i,2},\ \ldots\ E_{i,1023})^{\mathrm{T}}$. Unlike conventional quantitative EDXRF methods, the FSLS method directly relates element concentrations to the detected EDXRF spectrum. Therefore, it is able to establish the response relationship between the theoretical spectrum and the actual detected spectrum, which can be described in the following form:

$$\begin{pmatrix} E_{1,0} & E_{2,0} & \ldots & E_{i,0} \\ E_{1,1} & E_{2,1} & \ldots & E_{i,1} \\ E_{1,2} & E_{2,2} & \ldots & E_{i,2} \\ \vdots & \vdots & & \vdots \\ E_{1,1023} & E_{2,1023} & \ldots & E_{i,1023} \end{pmatrix} \cdot \begin{pmatrix} C_1 \\ C_2 \\ \vdots \\ C_i \end{pmatrix} = \begin{pmatrix} A_1 \\ A_2 \\ A_3 \\ \vdots \\ A_{1023} \end{pmatrix}. \tag{11}$$

This equation can be simplified as follows:

$$P_0 \cdot C_x = P. \tag{12}$$

Here, P_0 represents the theoretical pure-element matrix with a number of rows equal to the number of channels in the full spectrum and a number of columns equal to the number of pure elements of interest in the unknown sample. Matrix C_x consists of the calculated contents of the corresponding elements, which are updated after each iteration. P is the actual full spectrum measured with a portable EDXRF spectrometer. This instrument uses a Rh-

anode X-ray tube with a tube voltage of 30 kV. A Si-PIN semiconductor detector with a resolution of 196 eV (at ^{55}Fe) was employed. The measuring time was 300 s for each sample. The overdetermined equations presented in Eq. (11) have a unique smallest least-squares solution, which can be referred to in previous literature [26, 27]. The determination of factor G_i and each mass absorption coefficient will be described in detail in the next section.

3 Experiments

Determining factor G_i and the mass absorption coefficients is the key issue in the entire algorithm. As shown in Eq. (5), factor G_i can be seen as a structural constant for one specific element i in a certain detector system. However, it is difficult to directly calculate it. Replacing the absolute X-ray intensity with the relative intensity is the most common method to eliminate some physical parameters, including factor G_i [2, 28]. In this paper, a more innovative approach is proposed to calculate G_i with standard single-element samples through Eq. (6) and then to establish a function of G_i with the characteristic X-ray energy of different elements. Nine kinds of standard single-element (K, Ca, Ti, Fe, Ni, Zn, Sr, Zr, and Mo) samples with five different contents (9×5=45) were prepared in our laboratory. The component proportions of the 45 samples are listed in Table 1.

Here, SiO_2 was used as the matrix in the sample and H_3BO_3 was used as an adhesive for different contents. The G_i profile versus the characteristic X-ray energies of K, Ca, Ti, Fe, Ni, Zn, Sr, Zr, and Mo is shown in Fig. 4.

As shown in Fig. 4, the fitted formula between factor G_i and the characteristic X-ray energy E is:

$$G_i = 2 \times 10^6 E^{-1.393}. \tag{13}$$

The square of the correlation coefficient (R^2) is 0.9721. Therefore, the G_i factor of any element between K and Mo can be calculated via interpolation from Eq. (13). The mass absorption coefficient is another basic parameter that is closely related to the contents of unknown elements. The matrix information of the sample is the key to obtain the mass attenuation coefficient in EDXRF. In fact, the interaction of X-ray with compounds or mixtures along their trajectories can be equivalent to their interaction with single elements. The atomic number of this equivalent element is called the effective atomic number of this compound or mixture. Maynerod [29] first proposed a formula to calculate the effective atomic number Z_{eff}, which is given as follows:

$$Z_{\text{eff}} = \sqrt[m]{\sum f_i Z_i^m}. \tag{14}$$

Here, Z_i is the atomic number of element i in the irradiated matter and f_i is the electron percentage of element i in the

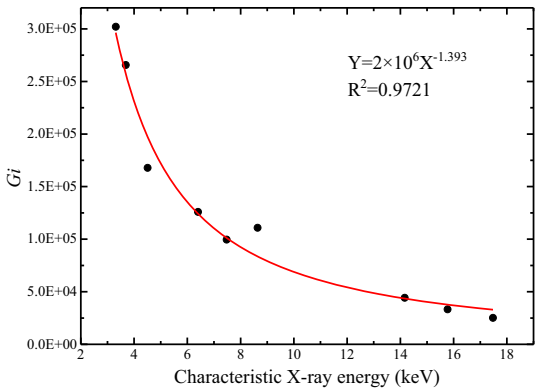

Fig. 4 (Color online) Relationship between factor G_i and the characteristic X-ray energies of different elements

irradiated matter. Index "m" is 2.49. Zhang et al. [13] divided the elements in a multi-component sample into two groups, including the known one and the "dark matrix." XZ_{eff} is defined to represent the effective atomic number of the "dark matrix." Thus, the calculation formula of Z_{eff} for a multi-component sample can be expressed as follows:

$$Z_{\text{eff}}^{2.94} = \sum C_i Z_i^{2.94} + (1 - \sum C_i) XZ_{\text{eff}}^{2.94}, \tag{15}$$

where C_i is the concentration of element i. Figure 5 is the actual X-ray spectrum of sample No. 11, obtained with the EDXRF spectrometer. The blue line stands for the raw X-ray spectrum. After smoothing and deducing background scattering (red line), the net X-ray spectrum (black line) can be obtained.

Rayleigh and Compton scattering peaks exist in the net EDXRF spectrum. Many researchers have concluded that the coherent-to-Compton scattering cross-sectional ratio depends only on the effective atomic number of composite materials [30]. Duvauchelle et al. [31] pointed out that a

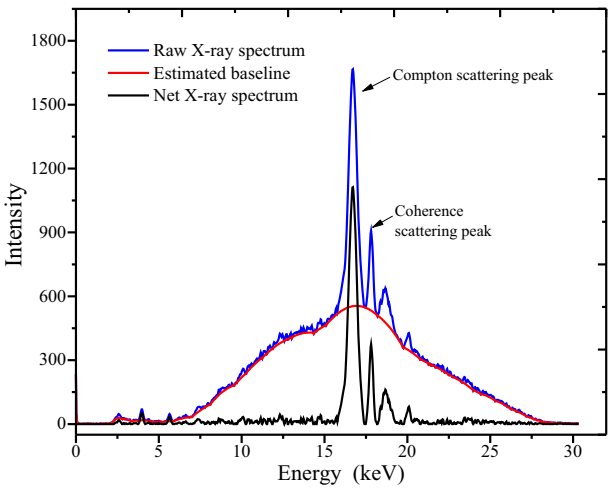

Fig. 5 (Color online) Actual X-ray spectrum of sample No. 11 (for a test time of 300 s)

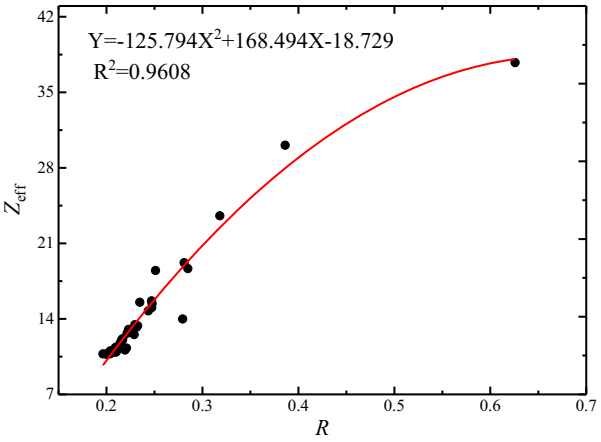

Fig. 6 (Color online) Relationship between R and Z_{eff} for different elements

given Z_{eff} should define a mixture or compound based on the intensity ratio of the Rayleigh-to-Compton scattering. İçelli et al. [32] successfully applied the coherent-to-Compton scattering cross-sectional ratio to obtain the Z_{eff} of some elements ($26 \leq Z \leq 82$). Thus, in this paper, we define R as the ratio of the coherence-to-Compton scattering net peak. As shown in Fig. 6, the functional relationship between Z_{eff} and R for different elements can be established as follows.

The relationship between Z_{eff} and R is fitted with a quadratic equation, as shown in Eq. (16).

$$Z_{\text{eff}} = -125.794R^2 + 169.494R - 18.729. \quad (16)$$

The square of the correlation coefficient is 0.9608. The mass absorption coefficient for a multi-component sample is equal to the sum of the weighted mass absorption coefficient of each component, including the known contents and the "dark matrix." This parameter can be derived [14] as follows:

$$\mu_{\text{S,E}} = \sum C_i \mu_{i,E} + (1 - \sum C_i)\mu_{XZ_{\text{eff}},E}. \quad (17)$$

Here, C_i is the concentration of element i, which should be updated after each iteration of Eq. (11). XZ_{eff} is the effective atomic number of the "dark matrix," whose mass absorption coefficient is defined as $\mu_{XZ_{\text{eff}},E}$. Related parameters and formulas for calculating the mass absorption coefficients can be referred to in the cross-sectional manual [33]. $(1 - \sum C_i)$ is the concentration proportion of the unknown "dark matrix." It should be noted that each mass absorption coefficient will be updated and the P_0 matrix will be reconstituted after each iteration. A simplified flow diagram of the whole algorithm can be drawn as shown in Fig. 7.

Fig. 7 Simplified flow diagram of the whole algorithm

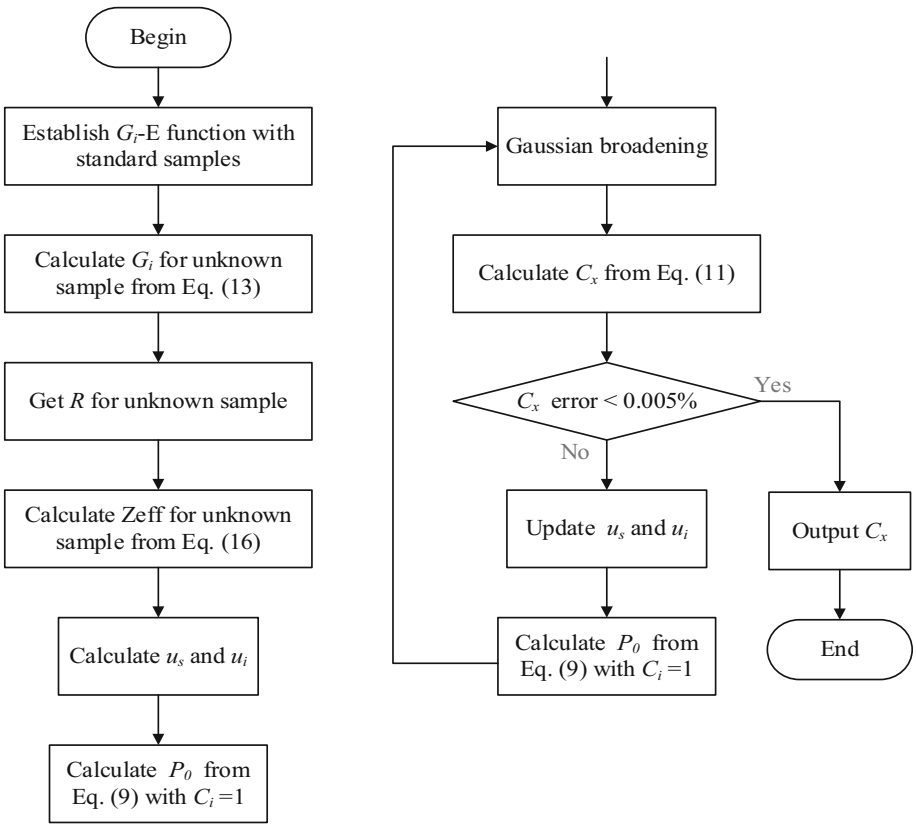

Table 2 Calculated results and relative errors for elements Ti, Fe, Ni, Cu, and Zn, out of the 13 Nss samples

Nss	Ti			Fe			Ni
No.	Standard content (%)	Calculated content (%)	Relative error (%)	Standard content (%)	Calculated content (%)	Relative error (%)	Standard content (μg/g)
2	0.271 ± 0.008	0.204 ± 0.014	25	2.462 ± 0.070	2.003 ± 0.071	19	19.4 ± 1.3
3	0.224 ± 0.008	0.190 ± 0.011	15	1.399 ± 0.050	1.243 ± 0.011	11	12.0 ± 2.0
4	1.080 ± 0.031	0.975 ± 0.095	10	7.205 ± 0.110	6.993 ± 0.046	3	64.0 ± 5.0
5	0.629 ± 0.021	0.657 ± 0.094	4	8.828 ± 0.180	8.859 ± 0.772	0	40.0 ± 4.0
6	0.439 ± 0.012	0.413 ± 0.055	6	5.659 ± 0.130	5.558 ± 0.029	2	53.0 ± 4.0
8	0.380 ± 0.012	0.298 ± 0.021	22	3.134 ± 0.050	2.865 ± 0.019	9	31.5 ± 1.8
9	0.424 ± 0.023	0.386 ± 0.034	9	3.358 ± 0.100	3.479 ± 0.035	4	33.0 ± 3.0
10	0.427 ± 0.006	0.383 ± 0.052	10	2.917 ± 0.030	3.029 ± 0.022	4	26.0 ± 1.0
12	0.392 ± 0.006	0.313 ± 0.029	20	3.295 ± 0.040	3.017 ± 0.028	8	32.0 ± 1.0
13	0.382 ± 0.011	0.295 ± 0.015	23	2.875 ± 0.040	2.480 ± 0.030	14	28.5 ± 1.2
14	0.466 ± 0.013	0.366 ± 0.023	21	3.722 ± 0.060	3.746 ± 0.007	1	33.0 ± 2.0
15	0.527 ± 0.020	0.451 ± 0.048	14	4.505 ± 0.070	4.104 ± 0.538	9	41.0 ± 1.0
16	0.578 ± 0.026	0.497 ± 0.045	14	3.805 ± 0.050	3.693 ± 0.026	3	27.4 ± 0.9

Ni		Cu			Zn		
Calculated content (μg/g)	Relative error (%)	Standard content (μg/g)	Calculated content (μg/g)	Relative error (%)	Standard content (μg/g)	Calculated content (μg/g)	Relative error (%)
61.6 ± 4.6	218	16.3 ± 0.9	22.9 ± 1.6	40	42 ± 3	70 ± 6	67
47.1 ± 1.2	293	11.4 ± 1.1	13.4 ± 0.8	18	31 ± 3	53 ± 4	70
113.0 ± 3.0	76	40.0 ± 3.0	55.6 ± 3.7	39	210 ± 13	259 ± 14	23
101.6 ± 8.0	154	144.0 ± 6.0	133.7 ± 25.6	7	494 ± 25	592 ± 69	20
107.2 ± 13.5	102	390.0 ± 14.0	424.2 ± 18.2	9	97 ± 6	124 ± 8	28
64.5 ± 5.5	105	24.3 ± 1.0	32.7 ± 1.6	35	68 ± 4	104 ± 8	54
88.3 ± 5.4	168	25.0 ± 3.0	31.1 ± 1.6	24	61 ± 5	103 ± 5	69
62.5 ± 4.0	141	19.0 ± 1.0	22.3 ± 0.3	17	60 ± 4	95 ± 12	58
77.1 ± 5.0	141	29.0 ± 1.0	40.6 ± 1.9	40	78 ± 5	117 ± 13	50
65.5 ± 4.3	130	21.6 ± 0.8	27.5 ± 1.4	28	65 ± 3	97 ± 5	50
73.3 ± 5.6	122	27.4 ± 1.0	37.2 ± 1.86	36	96 ± 3	142 ± 7	48
83.7 ± 2.1	104	37.0 ± 2.0	45.7 ± 1.38	23	94 ± 4	139 ± 16	48
80.7 ± 4.0	195	32.0 ± 2.0	34.9 ± 2.06	9	100 ± 8	149 ± 10	49

4 Results and discussion

In this paper, 13 national standard soil (Nss) samples were used to verify the feasibility of the FSLS algorithm. The iterations stop when the difference between the current and the former calculated contents is less than 0.005%. The results of the algorithm are given in Table 2.

Ti, Fe, Ni, Cu, and Zn were the most common elements in the geological samples. From Table 2, Ti and Fe, whose concentration exceeded several thousands of ppm, were labeled using percentage symbols (%), whereas the unit used for Ni, Cu, and Zn was micrograms per gram (μg/g). It is clear that the calculated contents for high-concentration elements are close to the standard contents. In particular, the calculated results for Fe are in good agreement with the standard contents and the corresponding relative errors are comparatively lower than those of the low-concentration elements. To intuitively analyze the trend changes in the content of each element, the resulting data were plotted as column graphs, with the error bars [34] representing standard deviation, in Fig. 8. The red columns stand for the standard contents, and the shadow columns represent the calculated contents. The blue line is the relative error level.

As shown in Fig. 8, the calculated content has the same variation tendency as the standard content among the 13 Nss samples, which reflects the feasibility of using the FSLS algorithm. There is a close relationship between the calculated content and the standard content except for Ni,

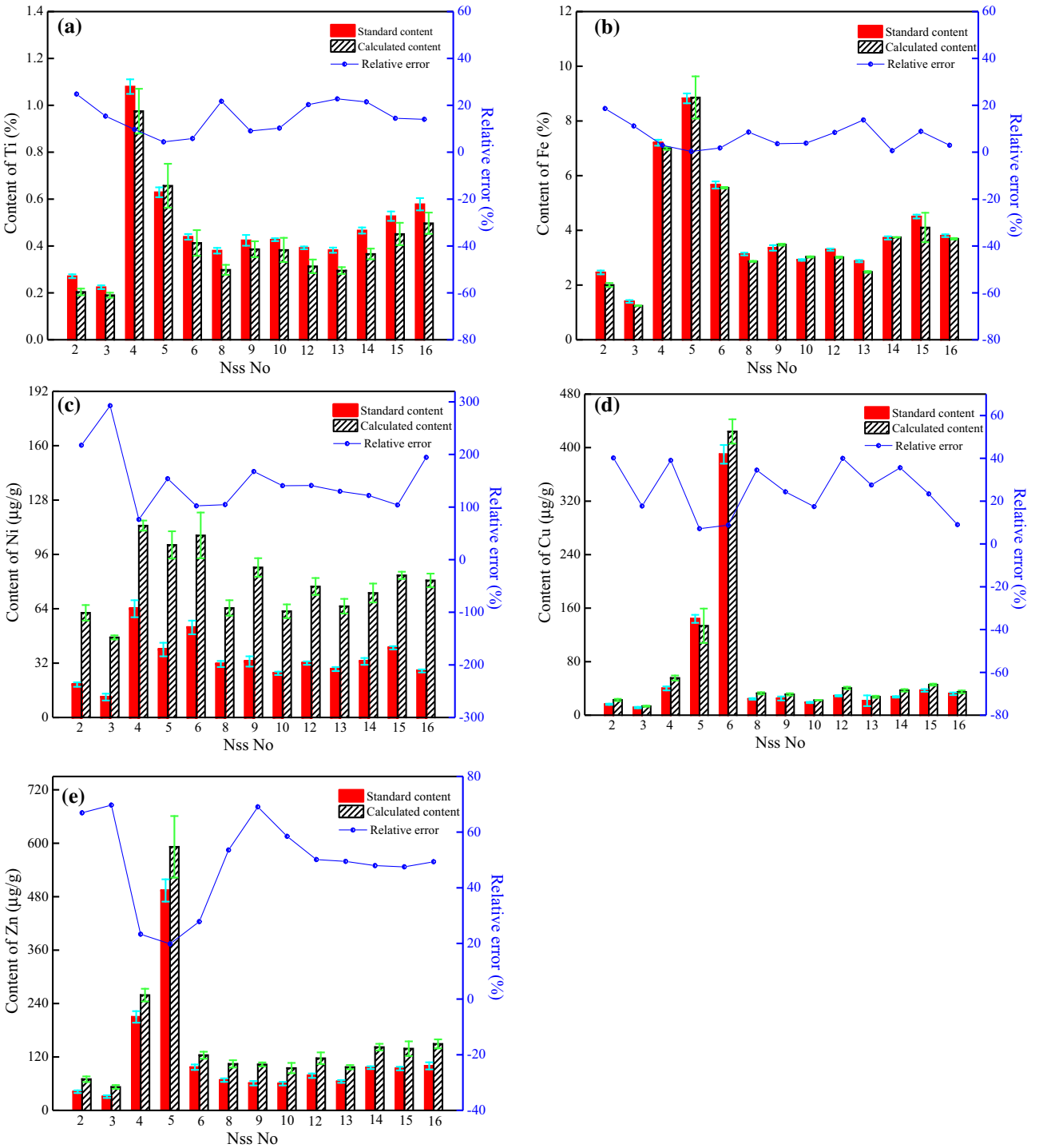

Fig. 8 (Color online) Column charts showing calculated content and standard content for elements **a** Ti, **b** Fe, **c** Ni, **d** Cu, and **e** Zn

whose relative error is larger than 100%. The analysis results are as follows.

(1) For high-concentration elements, such as Fe (as shown in Fig. 8b), whose maximum standard content is 8.828%, the minimum relative error is 0.35% (Nss 5). However, the relative error increases with the decrease in its standard content. When the standard content is 2.462%, the relative error reaches 18.64% (Nss 2), which is acceptable in EDXRF analyses. This is mainly because Fe is the major element in the solid samples; its concentration exceeds 1.39%. The background scattering intensity of the original X-ray beam can be considered inversely proportional to the

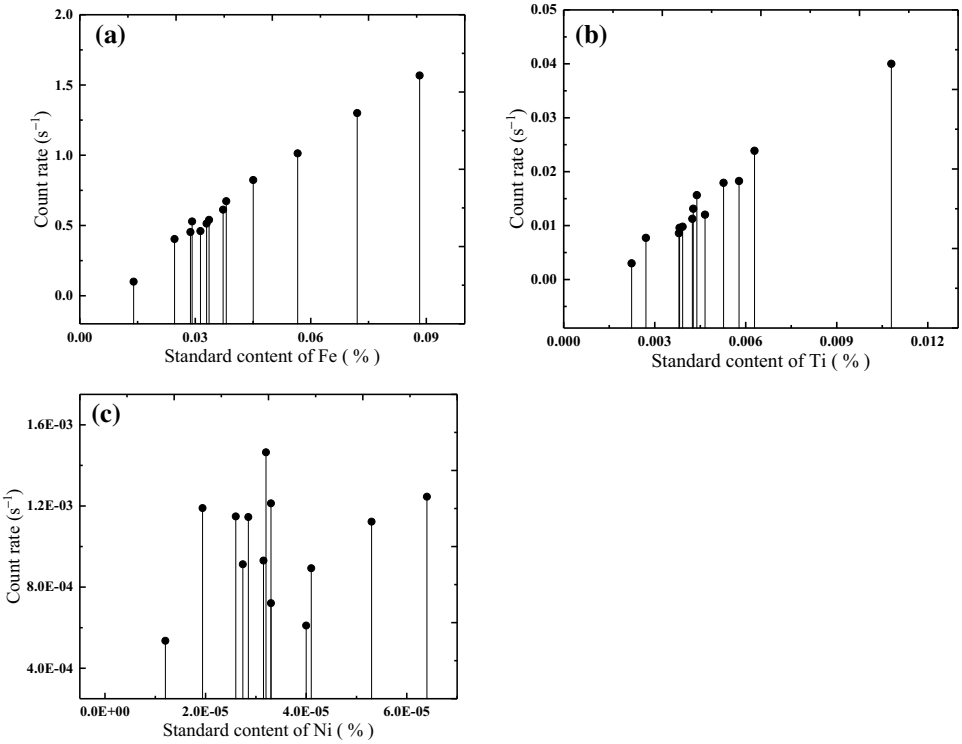

Fig. 9 Linear relationship between the count rate of the detector and the standard content of **a** Fe, **b** Ti, and **c** Ni

element contents. Therefore, comparatively low backscattered radiation contributes little to the characteristic peak area of Fe during the background-deducing step. In addition, the count rate of the detector is proportional to the content of Fe, as shown in Fig. 9a. Increasing the count rate would effectively reduce the statistical error. The calculation results of Ti, which is also a major element in the Nss samples, are similar to those of Fe. The differences between the red columns and the shadow columns for Ti in Fig. 8a exist for the same reason as for Fe.

(2) Ni, Cu, and Zn are microelements in the 13 Nss samples because their average contents are just 33.91 μg/g, 62.85 μg/g, and 115.08 μg/g, respectively. Their actual characteristic X-ray peaks are probably affected by the high backscattered radiation. As shown in Fig. 8c–e, the shadow columns of the calculated contents for these elements are almost higher than the red columns of their standard contents. This may be due to the absorption enhancement effects of other trace elements, such as Ce, Ba, and Pb, which leads to the actual characteristic X-ray intensity line deviating from the true intensity line. Among the 13 Nss samples, the one with a high content of Ni, Cu, and Zn has a smaller relative error than the other samples. The differences found between them are significantly related to measurement accuracy.

(3) However, for microelement Ni and as shown in Fig. 8c, the maximum relative error is 292.69%, which corresponds to 12 μg/g (Nss 3), and the minimum relative error is 76.49%, which corresponds to 64 μg/g (Nss 4). The average error is up to 149.80%, and the reason for this is not just related to the trace amount of Ni in the solid samples. Except for the absorption enhancement effect of the other microelements (which are neglected in this FSLS algorithm), the peak overlap effect caused by the elements (such as Co) adjacent to Ni is another main factor. Besides, the net characteristic X-ray intensity of Ni is heavily affected by the characteristic K_β rays of Fe, which are beyond the resolution capability of our detector. This leads to a strong increase in the weak peak area of the characteristic X-ray for Ni, and thus, the calculated content of Ni is far in excess of the standard value. The former can be used to calibrate the inter-element effects via empirical coefficient approaches and, in the subsequent step, increasing the number of the spectral variables in the P_0 matrix will, to some extent, reduce the mutual interference between elements. Furthermore, as shown in Fig. 9c, there is a nonlinear relationship between the content of the Ni element and the counting rate of the system. Therefore, statistical fluctuations during the spectral data acquisition will seriously influence the final calculated results. It is crucial to improve the accuracy of detection systems.

In addition, a single residual matrix is needed to optimize the FSLS algorithm, which can effectively modify the mismatch between the algorithm model and the X-ray characteristic spectrum data caused by statistical fluctuations, backscattered radiation, etc.

5 Conclusion

This paper introduces an FSLS method to quantitatively perform EDXRF analysis for unknown solid samples. Compared with the conventional FPM approach, it is a multivariate calibration method that is able to increase component selectivity and provide the possibility of detecting a sample as an outlier. The G_i factor and mass absorption coefficients are critical parameters to describe the features of the fluorescence spectra of pure elements. It is innovative to obtain the G_i factor for different elements through a $G_i - E$ function. To take full account of the unknown components in the sample, XZ_{eff} can be used to represent the effective atomic number of the "dark matrix." The coherent-to-Compton scattering peak ratio is applied to obtain the Z_{eff} of some of the elements. Based on fluorescence formulas, the calculated X-ray intensity should be Gaussian-broadened at the peak position to the scale edge (0–1023 channels) of the spectrometer. Subsequently, the response relationship between the theoretical spectral matrix and the actual X-ray spectrum can be established. The results show that using the FSLS method is feasible for light elements ($\geq$ hundreds of μg/g) in unknown samples. However, for microelements, high backscattered radiation, measurement accuracy, and inter-elements effects are the main sources of relative errors. In particular, for Ni, the characteristic K_β rays of Fe affect its weak characteristic X-ray peak. In future researches, increasing the number of the spectral variables in the P_0 matrix and optimizing the FSLS algorithm with a residual matrix will, to some extent, modify the mismatch between the algorithm model and the X-ray data and reduce the mutual interference between elements.

References

1. F. Cheng, Q.X. Zhang, L.Q. Ge et al., The study of advanced fundamental parameter method in EDXRF. Spectrosc. Spect. Anal. **35**, 2034–2037 (2015). https://doi.org/10.3964/j.issn.1000-0593(2015)07-2034-04. **(in Chinese)**
2. G.Y. Tao, S.J. Zhuo, A. Ji et al., An attempt at improving the accuracy of calculated relative intensities from theory in X-ray fluorescence spectrometry. X-ray Spectrom. **27**, 357–366 (1998). https://doi.org/10.1002/(SICI)1097-4539(199811/12)27:63.0.CO;2-P
3. Z.L. Dai, L.Q. Ge, D.H. Zou, The research of fundamental parameters method in energy dispersive X-ray fluorescence analysis. Nucl. Electron. Detect. Technol. **28**, 146–149 (2008). https://doi.org/10.3969/j.issn.0258-0934.2008.01.037. **(in Chinese)**
4. M. Liu, X.G. Tuo, Z. Li et al., The application of fundamental parameters method in EDXRF based on SDD. Nucl. Electron. Detect. Technol. **32**, 1096 (2012). https://doi.org/10.3969/j.issn.0258-0934.2012.09.024. **(in Chinese)**
5. M. Liu, X.G. Tuo, Z. Li et al., The application of fundamental parameters method in EDXRF based on SDD. Nucl. Electron. Detect. Technol. **32**, 1192–1195 (2012). https://doi.org/10.3969/j.issn.0258-0934.2012. **(in Chinese)**
6. J.W. Criss, *Fundamental-Parameters Calculations on a Laboratory Microcomputer* (Springer US, New York, 1980), pp. 93–97
7. J.W. Criss, L.S. Birks, Calculation methods for fluorescent X-ray spectrometry. Empirical coefficients versus fundamental parameters. Anal. Chem. **40**, 1080–1086 (1968). https://doi.org/10.1021/ac60263a023
8. V.Y. Borkhodoev, Accuracy of the fundamental parameter method for X-ray fluorescence analysis of rocks. X-ray Spectrom. **31**, 209–218 (2002). https://doi.org/10.1002/xrs.528
9. J.W. Criss, L.S. Birks, J.V. Gilfrich, Versatile X-ray analysis program combining fundamental parameters and empirical coefficients. Anal. Chem. **50**, 33–37 (1978). https://doi.org/10.1021/ac50023a013
10. K.K. Nielson, Matrix corrections for energy dispersive-X-ray fluorescence analysis of environmental samples with coherent-incoherent scattered X-ray. Anal. Chem. **49**, 641–648 (1977). https://doi.org/10.1021/ac50012a034
11. D. Wegrzynek, A. Markowicz, E. Chinea-Cano, Application of the backscatter fundamental parameter method for in situ element determination using a portable energy-dispersive X-ray fluorescence spectrometer. X-ray Spectrom. **32**, 119–128 (2003). https://doi.org/10.1002/xrs.626
12. R.E.V. Grieken, A.A. Markowicz, *Handbook of X-ray spectrometry* (Marcel Dekker, New York, 2002), pp. 151–179
13. Q.X. Zhang, Y.L. Guo, H.T. Bai et al., Determination of effective atomic numbers and mass attenuation coefficients of samples using in situ energy-dispersive X-ray fluorescence analysis. X-ray Spectrom. **47**, 4–10 (2018). https://doi.org/10.1002/xrs.2799
14. H.T. Bai, L.Q. Ge, Q.X. Zhang et al., The algorithm study on the EDXRF analysis of unknown sample content without using standard samples. J. Isotopes **31**, 14–19 (2018). https://doi.org/10.7538/tws.2017.youxian.028. **(in Chinese)**
15. F. He, V.S. Pierre, An integrated system for quantitative EDXRF analysis based on fundamental parameters. Nucl. Instrum. Methods A **299**, 580–583 (1990). https://doi.org/10.1016/0168-9002(90)90848-Z
16. J. Swerts, P.V. Espen, P. Geladi, Partial least-squares techniques in the energy-dispersive X-ray-fluorescence determination of sulfur graphite mixtures. Anal. Chem. **65**, 1181–1185 (1993). https://doi.org/10.1021/ac00057a013
17. P. Lemberge, P.J.V. Espen, Quantitative energy-dispersive X-ray fluorescence analysis of liquids using partial least-squares regression. X-ray Spectrom. **28**, 77–85 (1999). https://doi.org/10.1002/(sici)1097-4539(199903/04)28:2%3c77:aid-xrs312%3e3.3.co;2-3
18. F.S. Li, R.P. Gardner, W.J. Guo, Implementation of the Monte Carlo—library least-squares method to energy dispersive X-ray fluorescence analysis. Adv. X-ray Anal. (2013). https://doi.org/10.1016/j.apradiso.2011.09.012
19. P. Urbanski, E. Kowalska, Application of partial least-squares calibration methods in low-resolution EDXRS. X-ray Spectrom. **24**, 70–75 (1995). https://doi.org/10.1002/xrs.1300240209

20. J. Sherman, The theoretical derivation of fluorescent X-ray intensities from mixtures. Spectrochim. Acta **7**, 283–306 (1955). https://doi.org/10.1016/0371-1951(55)80041-0
21. T. Shiraiwa, N. Fujino, Theoretical calculation of fluorescent X-ray intensities in fluorescent X-ray spectrochemical analysis. J. Appl. Phys. **5**, 886–899 (1966). https://doi.org/10.1143/jjap.5.886
22. A.S.E. Santo, F.G. Wasserman, C.C. Conti, HPGe well detector calibration procedure by MCNP5 Monte Carlo computer code. Ann. Nucl. Energy **46**, 213–217 (2012). https://doi.org/10.1016/j.anucene.2012.03.037
23. R.A. Couture, R.F. Dymek, A reexamination of absorption and enhancement effects in X-ray fluorescence trace element analysis. Am. Miner. **81**, 639–650 (1996). https://doi.org/10.2138/am-1996-5-611
24. F.L. Li, X.J. Zhang, R.B. Wang, The determination method of MCNP Gaussian broadening coefficient and validation. Nucl. Electron. Detect. Technol. **33**, 1266–1270 (2013). https://doi.org/10.3969/j.issn.0258-0934.2013.10.024. **(in Chinese)**
25. Z. Li, X.G. Tuo, M. Liu et al., Monte Carlo simulation and Gaussian broaden technique for full energy peak of characteristic X-ray in EDXRF. Nucl. Tech. **35**, 911–915 (2012). **(in Chinese)**
26. Q.Y. Li, *Numerical Analysis* (Tsinghua University Press, Beijing, 2001), pp. 161–268. **(in Chinese)**
27. M.G. Cox, The least-squares solution of overdetermined linear equations having band or augmented band structure. IMA. J. Numer. Anal. **1**, 3–22 (1981). https://doi.org/10.1093/imanum/1.1.3
28. R.M. Rousseau, Fundamental algorithm between concentration and intensity in XRF analysis 1—theory. X-ray Spectrom. **13**, 115–120 (1984). https://doi.org/10.1002/xrs.1300130306
29. W. Maynerod, The significance of the Röntgen. Acta-Unio Internationalis Contra Cancrum **2**, 271–282 (1937)
30. P. Duvauchelle, G. Peix, D. Babot, Effective atomic number in the Rayleigh to Compton scattering ratio. Nucl. Instrum. Methods B **155**, 221–228 (1999). https://doi.org/10.1016/S0168-583X(99)00450-4
31. P. Duvauchelle, G. Peix, N. Freud et al., Tomographie par diffusion Rayleigh et Compton avec reconstruction numérique de l'image. J. Phys. IV Fr. **10**, Pr10435–Pr10448 (2000). https://doi.org/10.1051/jp4:20001046
32. O. Icelli, Practical method for experimental effective atomic number in the coherent to compton scattering ratio. J. Quant. Spectrosc. **101**, 151–158 (2006). https://doi.org/10.1016/j.jqsrt.2005.11.014
33. F. Biggs, R. Lighthill, Analytical approximations for X-ray cross sections III. Eur. J. Clin. Microbiol. **7**, 407–410 (1971). https://doi.org/10.2172/7124946
34. G. Cumming, F. Fidler, D.L. Vaux, Error bars in experimental biology. J. Cell Biol. **177**, 7–11 (2007). https://doi.org/10.1083/jcb.200611141